Geophysical Research Letters

Supporting Information for

Were the May 2012 Emilia-Romagna earthquakes induced? A coupled flow-geomechanics modeling assessment

R. Juanes[1,2], B. Jha[1†], B. H. Hager[2], J. H. Shaw[3], A. Plesch[3], L. Astiz[4‡], J. H. Dieterich[5], C. Frohlich[6]

[1] Department of Civil and Environmental Engineering, Massachusetts Institute of Technology, Cambridge, Massachusetts, USA

[2] Department of Earth, Atmospheric and Planetary Sciences, Massachusetts Institute of Technology, Cambridge, Massachusetts, USA

[3] Department of Earth and Planetary Sciences, Harvard University, Cambridge, Massachusetts, USA

[4] Institute of Geophysics and Planetary Physics, University of California San Diego, San Diego, California, USA

[5] Department of Earth Sciences, University of California Riverside, Riverside, California, USA

[6] Jackson School of Geosciences, University of Texas at Austin, Austin, Texas, USA

]

Contents of this file

Additional Supporting Information (Files uploaded separately)

Introduction

The supporting information gives details pertaining to the analysis of seismicity near the Cavone field injection well (Text S1, and Figures S1-S2) and the coupled flow and geomechanical modeling of the Cavone reservoir (Text S2, and Figures S3-S5), along with additional referenes (Text S3). It also includes movies with results from the coupled flow-geomechanical dynamic model showing the evolution of pressure (Movie S1) and change in Coulomb stress (Movie S2) at the Mirandola fault.

Text S1. Analysis of seismicity near the Cavone field injection well

This section summarizes instrumentally-recorded regional seismicity prior to and following the Emilia-Romagna 2012 earthquakes, focusing on activity occurring in the neighborhood of the Cavone well #14. We supplement already-published investigations [e.g., *Scognamiglio et al.*, 2012; *Lavecchia et al.*, 2012] with relocation of selected earthquakes near Cavone #14 occurring between 2001 and June 2012; these are especially well-recorded events, many recorded by seismograph stations managed by the Operator providing data not available to the International Seismological Centre (ISC). For these events we augmented phases reported by the ISC with data recorded by local stations, when these data were available. For these relocated hypocenters we have credible information about focal depths.

Seismic activity prior to 2012

Because the routine locations reported by the ISC and INGV may have large location errors, we have relocated a select group of events near Cavone well #14 (Fig. 2a,b in the main text). The phase data used for these relocations are a combination of P and S arrivals reported by the ISC, supplemented by P and S arrivals recorded at four stations (station codes ROCE, SGIA, ROVE and CORR) operated privately in the Cavone area. The Operator provided phase arrivals for 126 earthquakes occurring 2000-2012; of these 67 occurred between 2001 and 2011, and 59 occurred in May or June 2012 during the Emilia-Romagna sequence. Of the 2001-2011 earthquakes, 28 satisfied the requirement that the largest epicenter-to-station azimuthal gap among the recording stations was 200° or less. Essentially, these requirements constrain the location process, minimize systematic errors caused by incorrect assumptions about heterogeneities in the regional crustal structure, and make it possible to obtain reliable epicenters and focal depths. To determine the relocated epicenters we used the double-difference location method [*Waldhauser and Ellsworth*, 2000]. The double-difference method is designed to obtain accurate relative locations among a group of events from a restricted geographical area. By comparing the relative arrival times at individual stations for nearby events, it minimizes problems caused by errors in phase readings, and by the absence of readings at particular stations, even if the assumed crustal velocity model is inaccurate or if crustal velocity is heterogeneous. The resolution of the resulting locations generally is superior for identifying clusters, lineations or planar groups of earthquakes.

The majority of the 28 relocated hypocenters (green circles in Fig. 2a,b) that occurred years prior to the Emilia-Romagna 2012 sequence are within about 8 km of Cavone well #14. The proximity to the well is unsurprising since the selection procedure (i.e., selecting events recorded by local stations) favors events in or near the Cavone field. The focal depths range between 4.6 km and 10.3 km. In the approximately west-facing cross section (Fig. 2b in main text), they appear situated along a southward-dipping plane that is roughly coincident with one nodal plane of the 20 May 2012 earthquake. All but two of the relocated earthquakes occurred in the years 2004-2009.

Seismic activity during May-June 2012

The Emilia-Romagna earthquake sequence has properties of a cascading series of foreshocks and aftershocks common with tectonic earthquakes. It began with a mb 2.9 event on May 18. This event was followed on May 19 by three earthquakes with mb of 2.5, 4.2, and 2.2 respectively. The two principal events in the May 2012 Emilia-Romagna sequence had magnitudes Mw of 6.0 and 5.8 respectively, and occurred 20 May 2012 and 29 May 2012. Source modeling of the May 20 and 29 events indicate a complex source for the May 20

earthquake [*Cesca et al.*, 2012; *Piccinini et al.*, 2012] and possible static triggering of the May 29 event [*Ganas et al.*, 2012].

The 20 May Mw 6.0 event occurred at 0203 with an epicentral distance less than 3 km from the 19 May mb 4.2 foreshock and about 22 km from Cavone well #14. This event triggered a vigorous aftershock sequence (Fig. S1, top) with numerous epicenters clustered east of the well at distances of ~8-25 km (Fig. 2c in main text). During the 20-28 May time period virtually all the activity remained more than 8 km from the well.

The second Mw 5.8 earthquake sequence occurred at 0700 29 May 2012, beginning about 10 km east of well #14. The ISC-reported aftershock locations included numerous events with epicenters near Cavone well #14 (Fig. S1, bottom). There were also numerous events towards the east that appear to be continuing aftershocks of the 20 May event. After 29 May aftershocks extended westward up to 10-15 km from the well. In addition, there were several earthquakes with magnitudes between 3 and 4 at distances 15-30 km west of the well (Fig. 2c in the main text).

To obtain accurate locations and reliable focal depths, we relocated 41 selected earthquakes in the May-June 2012 sequence (red circles in Fig. 2a,b in the main text). The phase data used for these are a combination of P and S arrivals reported by the ISC, supplemented by data recorded at the four local Cavone stations. The selected events all were recorded by stations surrounding their epicenters such that no azimuthal gaps exceeded 120°. The relocated hypocenters occupy an approximately 15-km long planar east-west region situated beneath Cavone well #14. Focal depths ranged from 4.8 to 9.6 km.

Seismic activity during May 2012-June 2014

Since May 2012, aftershocks of the 20 May and 29 May 2012 earthquakes have continued into 2013 and 2014. The frequency of reported earthquakes between June 2012 and June 2013 was significantly higher than between 2005 and 2011. However, as is typical of aftershock sequences, the rates of seismic activity have been declining since June 2012 (Fig. S2).

Text S2. Coupled flow and geomechanical modeling of the Cavone reservoir

Structural and stratigraphic model

We developed a new reservoir model that includes the major stratigraphic and structural elements in the region, placing an emphasis on defining the precise structural relationships between the reservoir units and Mirandola fault so that the simulation and geomechanical modeling can examine how field operations might influence the fluid pressures and stresses acting on the fault. The top of the reservoir layer corresponds to the "Breccia top" and the base to the "Nor_B bottom" horizon. We extended these horizons away from the Cavone fold crest based on interpretation of 2-D seismic reflection data (Figs. S3 and S4). These seismic data were depth-converted using velocity functions based on sonic logs from the Cavone field. This mapping, guided by structural analysis, defined the structure of the forelimb of the Cavone anticline, which dips steeply (>50°) to the northeast and is cut by splays of the Mirandola fault.

We developed triangulated surface representations of the stratigraphic horizons and faults (Fig. 3a in the main text) that served as the basis for developing a hexahedral mesh that was used for the computations (Fig. 3b in the main text). We used the Trelis software (CUBIT, 2013) to generate the hexahedral grid that honors these three surfaces. Developing a regular, volumetric mesh for the structure was challenging given the steep bed dips and the cutoff relationships with the Mirandola fault. Thus, this process involved iteratively simplifying and smoothing the initial structural model in order to develop a mesh that would support the computational analysis.

Mathematical model of coupled flow and geomechanics

Here, we employ the computational model for coupled flow and geomechanics of faulted reservoirs. We couple a flow simulator with a mechanics simulator using the fixed-stress scheme [*Kim et al.*, 2011, 2013]. We employ a rigorous formulation of nonlinear multiphase geomechanics [*Coussy*, 1995] based on the increment in mass of fluid phases, instead of the more common, but less accurate, scheme based on the change in porosity. To account for the effect of surface stresses along fluid-fluid interfaces, we use the equivalent pore pressure in the definition of multiphase effective stress [*Coussy*, 1995]. We model faults as surfaces of discontinuity using interface elements [*Aagaard et al.*, 2013]. This allows us to model stick-slip behavior on the fault surface for dynamically evolving fault strength. The mathematical formulation of multiphase poromechanics, and the computational model, are described in detail elsewhere [*Jha and Juanes*, 2014].

Poromechanics of faults

A central feature of our work is that we treat faults as surfaces of discontinuity embedded in the continuum, across which displacement is allowed to be discontinuous to recognize the possibility of fault slip. We use the Mohr-Coulomb theory to define the stability criterion for the fault [*Jaeger and Cook*, 1979]. When the shear traction on the fault is below the friction stress, $\tau \leq \tau_f$, the fault does not slip. When the shear traction is larger than the friction stress, $\tau > \tau_f$, the contact problem is solved to determine the slip on the fault [*Aagaard et al.*, 2013].

Traditionally, in the Andersonian theory of faulting [*Anderson*, 1951], fault slip is modeled in a "dry environment," that is, in the absence of fluids. A difference in fluid pressure across the fault leads to a pressure jump between the "positive" and the "negative" sides of the fault. One of the key features of the 2-D representation of faults is the ability to reproduce a finite jump in the pressure across the fault. This pressure jump leads to a discontinuity in the effective stress across the fault, such that the total stress is continuous. Fault stability must be assessed by evaluating the stability criterion on both sides of the fault separately. The side of the fault where the criterion is met first determines the fault stability. We define a fault pressure as the maximum of the pressures on both sides of the fault, $p_f = \max(p_+, p_-)$. This definition of fault pressure is a natural result of our fault representation, rather than a conservative assumption [*Jha and Juanes*, 2014].

Simulation model

We consider a two-phase black-oil system with linear poroelasticity. The wells are operating within the reservoir layer; however, the coupled simulation is performed over the entire domain to account for the effect of flow on the stability of the fault. The fault is treated as impermeable to flow, however, we could perform sensitivity analysis later by changing the fault permeability values, both along and across the fault. Similarly, we can perform sensitivity on the strength of the aquifer support.

We initialize the pressures hydrostatically with a datum pressure of 290.1 bar (4207.5 psi) at a depth of 2990 m (9809.6 ft), oil density of 22 API gravity, and water density of 1000 kg/m^3. We initialize the saturations with an irreducible water saturation of 0.38 and a residual oil saturation of 0.17. We choose these values such that the model is able to honor the historical rates of production and injection for the prescribed porosity and permeability values.

Initial displacements are zero everywhere. Initial stresses compatible with reverse faulting conditions are prescribed to be lithostatic in the vertical direction, twice the lithostatic in north-south, and 1.5 times the lithostatic in the east-west direction. The lithostatic gradient is calculated with the bulk density, which depends on the solid grain density, assumed to be 2600 kg/m^3, fluid phase densities, fluid saturations, and porosity. We apply compression at twice the lithostatic on the northern boundary and apply roller boundary conditions on east, west, south, and bottom boundaries. The top boundary is a traction-free surface. All boundaries are no-flow boundaries.

For this study, we assume a uniform distribution of properties with values that are within the range of values used in a history match simulation from the Operator, and consistent with values inferred from the Cavone lab well test [*LabCavone*, 2014]: porosity = 0.1, permeability = 1 md, Young's modulus = 55 GPa, and Poisson's ratio = 0.28. We use the fluid PVT data (oil formation volume factor, and oil viscosity), and oil and water relative permeabilities shown in Fig. S5.

We perform the dynamic simulation from 1 March 1980 to 31 Dec 2012 (duration 11994 days) by imposing the historical oil production rate for producers and historical water injection rate for injectors. We include 19 Cavone wells in the flow model with their actual completion intervals and rates. All the wells are located near the crest of the Cavone anticline (Fig. 3a in the main text). Our simulation models the Cavone reservoir as having both lateral and bottom-aquifer support. For the overburden layers above the reservoir, we use a transmissibility multiplier in the vertical direction to isolate the reservoir from layers above it. There is evidence both from the permeability measurements in cores and from the temperature profile in the injection test as part of Cavone Lab that flow extends into the aquifer below the reservoir. Pressure changes extending to substantial depth beneath the reservoir makes the results from this model subtle to interpret. However, it is our preferred model because it is consistent with the constraints interpreted from the Cavone Lab interference test.

Bottom aquifer support leads to a relatively small pressure drop around the producers and pressure rise around the injectors. The pressure drops at the producing wells are close to the observed pressure drops, although the pressure increase predicted for injector Cavone #14 is smaller than that observed. This may be evidence for lateral heterogeneity in the permeability structure, consistent with the fall-off test of the Cavone Lab. A separate simulation that includes only lateral support predicts pressure drops around the injectors that are an order of magnitude larger than those measured in the field, suggesting that lateral pressure support only is insufficient to explain observations. In the simulation from our preferred model discussed here, pressure changes on the hanging-wall side of the Mirandola fault from production and injection propagate down into the support aquifer, but the magnitude of the pressure variations is relatively small (Fig. 3b in the main text).

Text S3. References

Aagaard, B. T., M. G. Knepley, and C. A. Williams, A domain decomposition approach to implementing fault slip in finite-element models of quasi-static and dynamic crustal deformation, *J. Geophys. Res. Solid Earth* 118, 3059-3079 (2013).

Anderson, E. M., *The Dynamics of Faulting and Dyke Formation With Application to Britain*, Oliver and Boyd, New York, N.Y. (1951).

Cesca, S., T. Braun, F. Maccaferri, L. Passarelli, E. Rivalta and T. Dahm, Source modeling of the M5-6 Emilia-Romagna, Italy earthquakes (2012 May 20-29), *Geophys. J. Int.* 193, 1658-1672 (2013).

Coussy, O., *Mechanics of Porous Continua*, John Wiley, Chichester, U.K. (1995).

CUBIT, CUBIT 13.2 User Documentation, Sandia Natl. Lab., Albuquerque, N.M. (2013).

Ganas, A., Z. Roumelioti and K. Chousianitis, Static stress transfer from the May 20, 2012, M 6.1 Emilia-Romagna (northern Italy) earthquake using a co-seismic slip distribution model, *Ann. Geophys.* 55, 655-662 (2012).

Jaeger, J. C., and N. G. W. Cook, *Fundamentals of Rock Mechanics*, Chapman and Hall, London, U.K. (1979).

Jha, B., and R. Juanes. Coupled multiphase flow and poromechanics: A computational model of pore pressure effects on fault slip and earthquake triggering, *Water Resour. Res.* 50(5), 3776-3808 (2014).

Kim, J., H. A. Tchelepi, and R. Juanes, Stability and convergence of sequential methods for coupled flow and geomechanics: Fixed-stress and fixed-strain splits, *Comput. Methods Appl. Mech. Engrg.* 200, 1591-1606 (2011).

Kim, J., H. A. Tchelepi, and R. Juanes, Rigorous coupling of geomechanics and multiphase flow with strong capillarity, *Soc. Pet. Eng. J.* 18(6), 1123-1139 (2013).

Laboratorio di Monitoraggio Cavone, Risultati del Programa di Prove (2014). Available at http://labcavone.it

Lavecchia, G., R. de Nardis, D. Cirillo, F. Brozzetti, and P. Boncio, The May-June Ferrara Arc earthquakes (northern Italy): Structural control of the spatial evolution of the seismic sequence and of the surface pattern of coseismic fracture, *Ann. Geophys.* 55, 534-540 (2012).

Piccinini, D., N. A. Pino and G. Saccorotti, Source complexity of the May 20, 2012 Mw 5.9, Ferrara (Italy) event, *Ann. Geophys.* 55, 568-573 (2012).

Scognamiglio, L., L. Margheriti, F. M. Mele, E. Tinti, A. Bono, P. De Gori, V. Lauciani, F. P. Lucente, A. G. Mandiello, C. Marcocci, S. Mazza, S. Pintore and M. Quintiliani, The 2012 Pianura Padana Emiliana seimic sequence: Locations, moment tensors and magnitudes, *Ann. Geophys.* 55, 549-559 (2012).

Toda, S., R. R. Stein, and T. Sagiya, Evidence from the 2000 Izu Islands swarm that seismicity is governed by stressing rate, *Nature* 419, 58-61 (2002).

Waldhauser, F., and W. L. Ellsworth, A double-difference earthquake location algorithm: Method and application to the northern Hayward fault, *Bull. Seismol. Soc. Amer.* 90, 1353-1368 (2000).

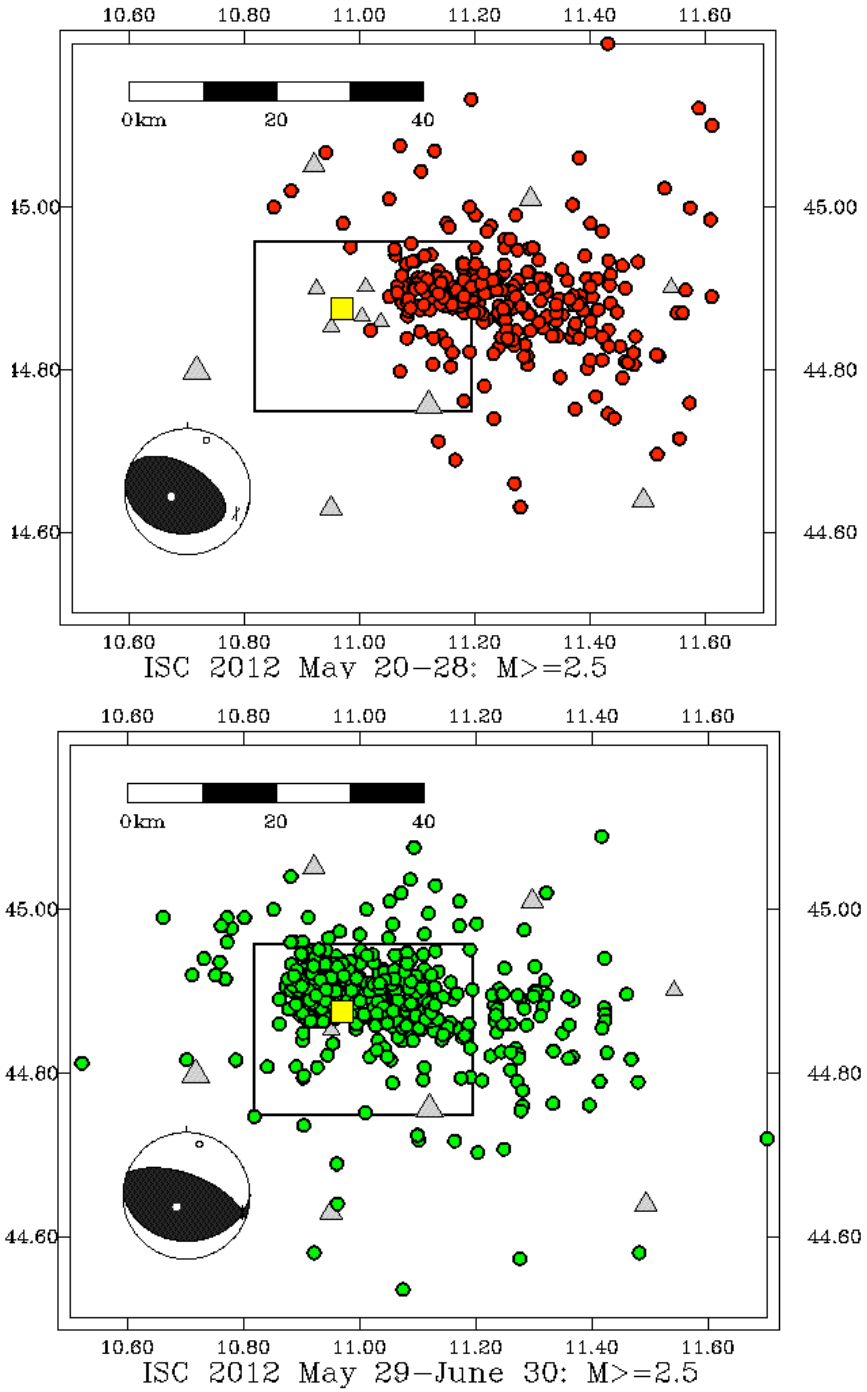

Figure S1. Maps with epicenters and aftershocks of large earthquakes occurring 20-28 May 2012 (top: red circles) and 29 May-30 June 2012 (bottom: green circles). Plotted epicenters have magnitudes of M2.5 and larger and are as reported by the ISC. Yellow square is Cavone well #14. Triangles are seismograph stations. Rectangle indicates region of the geomechanical model shown in Fig. 3 in the main text. Plotted focal mechanisms for both events are from the Global Centroid Moment Tensor (GCMT) catalog.

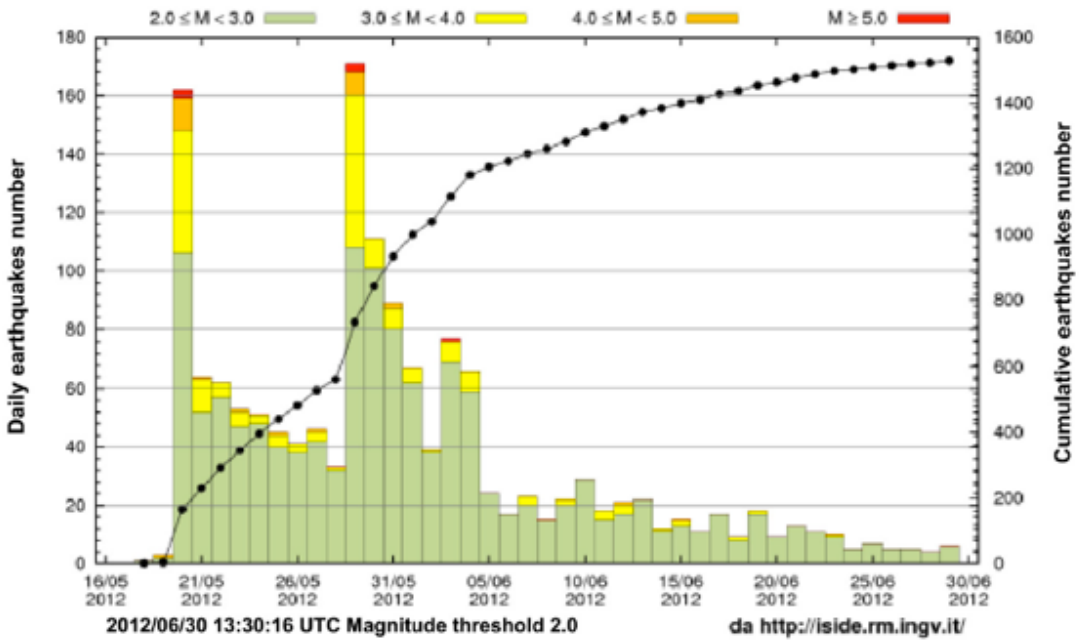

Figure S2. Plot of the daily number of earthquakes of various magnitudes through the Emilia-Romagna earthquake sequence. The record indicates three sudden increases in activity, followed by more gradual decreases, consistent with the view in which a sudden stress change causes an aftershock sequence that decays inversely with time [*Toda et al.*, 2002].

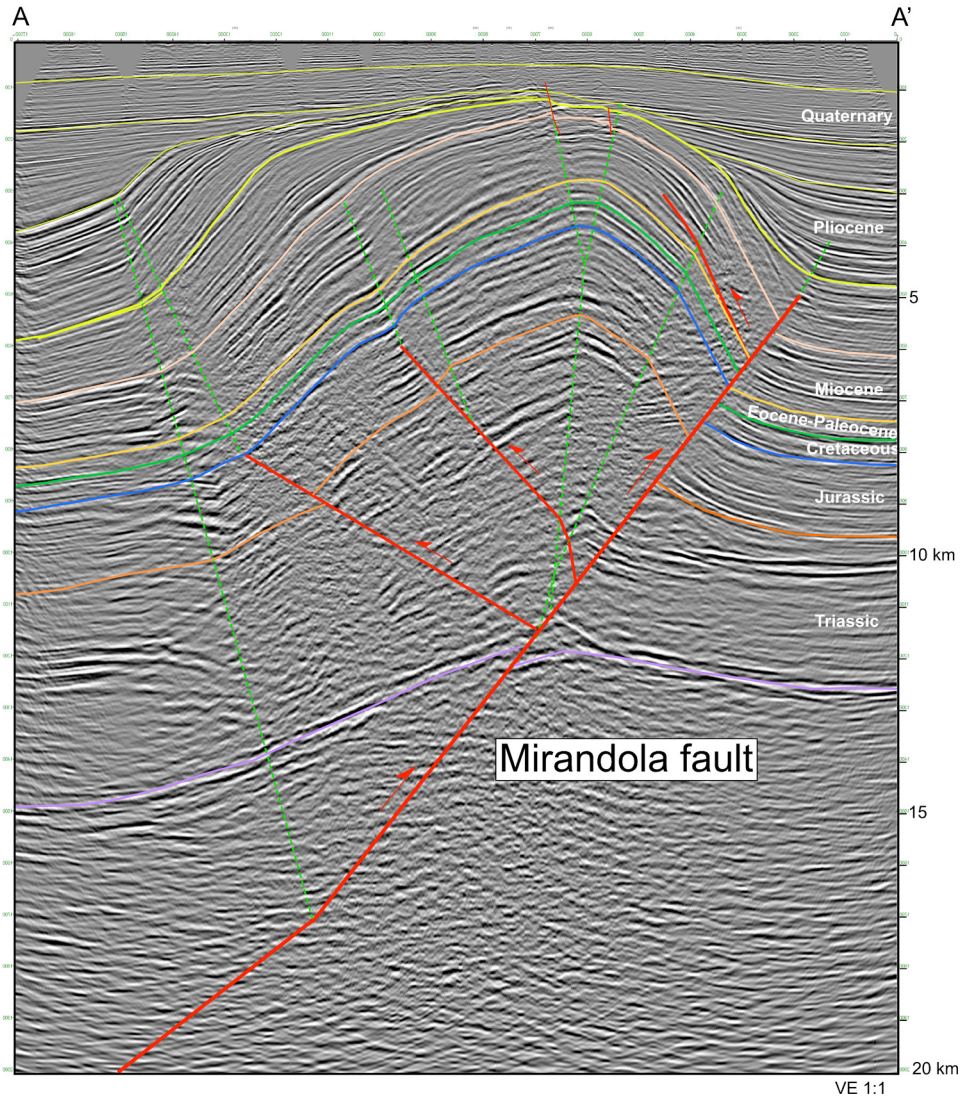

Figure S3. Migrated and depth converted seismic reflection profile showing location and geometry of the Mirandola fault and overlying anticline that provides trap for the Cavone oil field. "Breccia top" and "Nor_B bottom" horizon used in the reservoir model correspond approximatey to the top Jurassic and top Triassic horizons shown in this section. The Section trace A-A' is shown in Fig. S4.

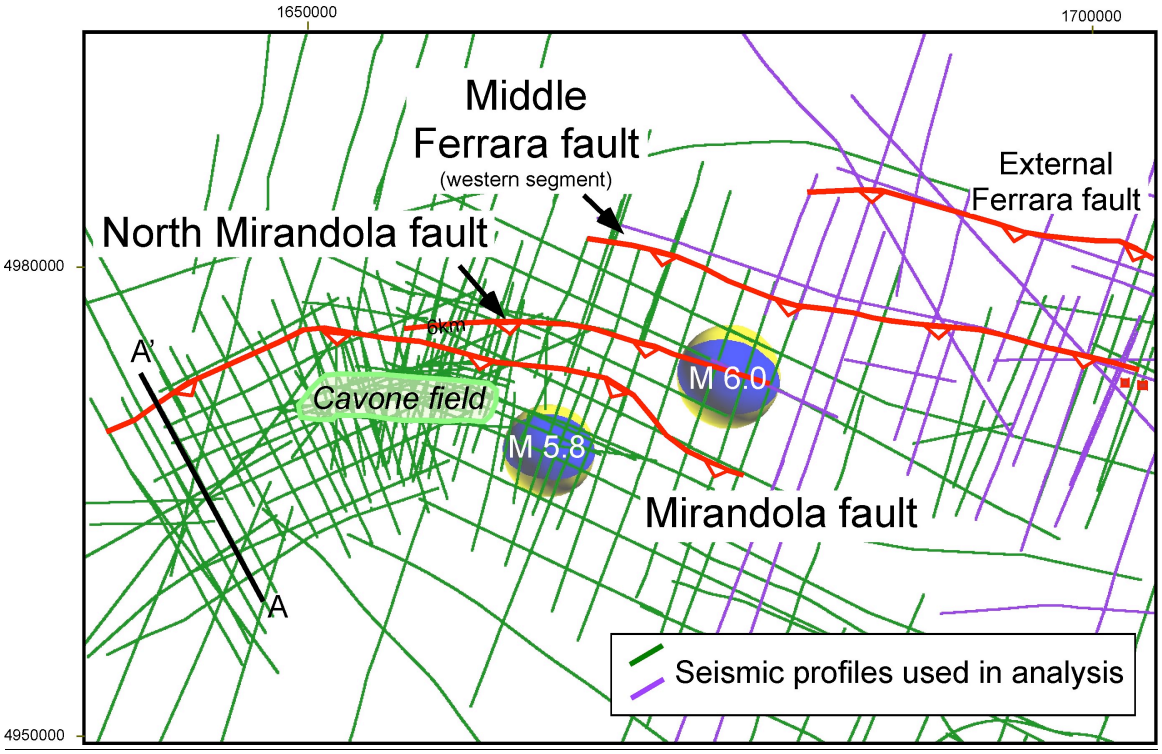

Figure S4. Base map showing locations of seismic profiles used to constrain the structural and stratigraphic model used in this analysis. The Section A-A' is shown in Fig. S3.

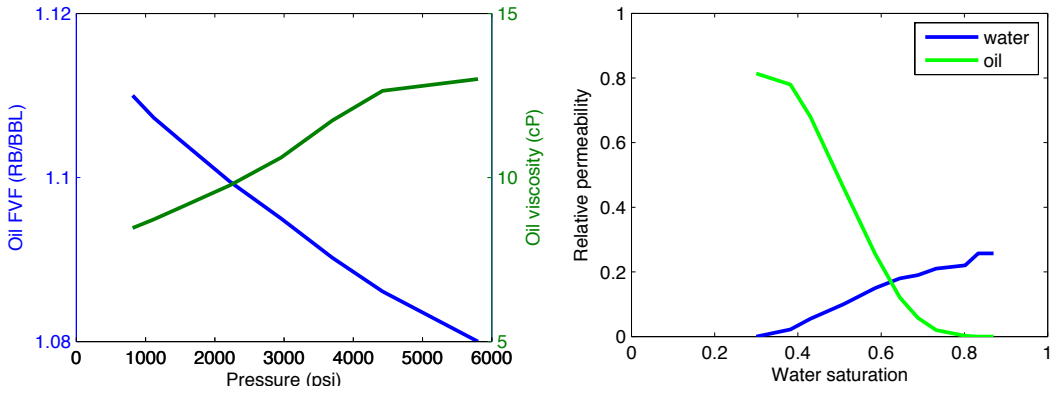

Figure S5. Multiphase-flow constitutive relations. Left: Oil formation volume factor and oil viscosity. Right: relative permeabilities.

Movie S1. Results from the coupled flow-geomechanical dynamic model. Evolution of the pore pressure (in bar) at the hanging-wall side of the Mirandola fault during the simulation period (March 1, 1980 – December 31, 2012). Red color indicates pressure build-up as a result of injection in the Cavone #14 well. Blue color indicates pressure decline as a result of fluid extraction, which extends into the underlying aquifer. The May 29, 2012 hypocenter location is shown with a circle.

Movie S2. Results from the coupled flow-geomechanical dynamic model. Evolution of the change in Coulomb stress, ΔCFF, on the Mirandola fault (in bar) during the simulation period (March 1, 1980 – December 31, 2012). The change in the effective normal traction is positive near producers and negative near injectors because pressure depletion leads to contraction of the reservoir and pressure increase leads to increased compression on the fault. The white cross mark on the ΔCFF plot denotes the hypocenter location of the May 29, 2012 earthquake.